Analyst

Accepted Manuscript

ROYAL SOCIETY OF CHEMISTRY

www.rsc.org/analyst

Trace detection of nitro aromatic explosives by highly fluorescent g-C_3N_4 nanosheets

Hai-Yu Chen,[a] Lin-Wei Ruan,[a] Xia Jiang, [a] Ling-Guang Qiu,[a,] *

[a] *Laboratory of Advanced Porous Materials, School of Chemistry and Chemical Engineering, Anhui University, Hefei 230601, China.*

* Corresponding author:

Fax: +86 551 65108212; Tel: +86 551 65108212;

E-mail: ahulgqiu@126.com (L. G. Qiu).

Abstract

Highly fluorescent g-C_3N_4 nanosheets were facilely fabricated by exfoliating the bulk g-C_3N_4 under ultrasonic irradiation for 1h. The atomic force microscopy (AFM) image showed that the resultant g-C_3N_4 nanosheets were ~6-14 nm thick, and the suspension could stably exist in air for several weeks. Remarkably, the obtained nanosheets exhibited strong fluorescence with extremely high quantum yield (QY) up to 32%, and high sensitivity, selectivity, as well as fast response to nitro aromatic explosives were observed. Typically, the quenching efficiency coefficient K_{sv} for PNP was 30460 M^{-1}, which proved the resultant nanosheets possessed extremely high sensitivity for nitro-phenol PNP detection.

1. Introduction

Rapid detection and analysis of explosives is necessary for forensic, environmental, and the national defense organization. Recently, there is a growing demand in rapid detection of nitro aromatic explosives (NACs) for their explosiveness, mutagenicity, carcinogenicity and environmental issues.[1, 2] NACs concentration in natural aqueous media is usually limited to trace levels at present stage. A sensitive strategy is therefore needed to detect these NACs. Presently, several methods including spectroscopy, electrochemical method, solid-phase micro-extraction-liquid chromatography, and fluorescence response method[3-5] are commonly used to detect these explosive chemicals. However, solid-phase micro-extraction-liquid chromate-graphy suffers from the weakly volatile explosives, while electrochemical sensing limit is too high to be applicable of trace level NACs. Fluorescence response strategy is very suitable for detecting trace level of NACs in principle with low cost, fast response, non-destructive, high selectivity and sensitivity.[6-8]

For the detection of explosives, a lot of materials, such as conjugated polymers, metal-organic frameworks, modified inorganic nanoparticle, nanoclusters and colloidal semiconductor nanocrystals[9-12] were reported for detecting these explosives. Among all these materials, conjugated polymers are especially attractive for their ability to produce signal gain in response to an interaction with target analytes. g-C_3N_4 is a kind of conjugated polymer, it is the most stable allotrope of carbon nitride and it could be prepared in large scale by polymerizing nitrogen-rich precursors involving dicyan-diamide, melamine, urea, and thiourea. g-C_3N_4 has been extensively used as a polymeric photo-catalyst for solar hydrogen production and environmental purification，as well as oxygen reduction and evolution.[13-16] However, few concerns on fluorescent property of bulk g-C_3N_4 has been reported as bulk g-C_3N_4 can hardly form stable suspension. Very recently, Zhang *etal.*[17] found that the g-C_3N_4 nanosheets had high performance of photoluminenscence, which opened another door for the application of g-C_3N_4. To date, although applications of g-C_3N_4 nanosheet in sensing of glucose and Cu^{2+} have been reported,[18-21] no report on detecting NACs using g-C_3N_4 nanosheets was found in literature.

Like graphite, g-C_3N_4 has a layered, planar structure. In each layer, the C and N atoms are covalently bonded, and the C-N layers stack together by the weak van der Waals force with a distance of 3.3 nm[22]. The ultrasonic wave is defined as the sound with the frequency beyond the range of human hearing, typically at 16 kHz. Ultrasonic wave energy could be transferred to heat and pressure.[23] Ultrasonic synthesis has been proved to be an effective technique for generating nanoparticles in short reaction time.[24, 25]

Our research group has reported some works on detection of NACs over fluorescence quenching of MOFs. Such as Fe_3O_4@Tb-BTC framework nano-spheres could be used for high sensitivity detection of 2,4,6-trinitrotoluene (TNT).[26] However, Fe_3O_4@Tb-BTC is high cost for

Tb is very expensive, and its synthetic controllability is not very good. Herein, the highly fluorescent g-C_3N_4 nanosheet (QY up to 32%, the detailed measurements is in supplementary information) was used as sensing material to detect the trace level NACs, such as nitrobenzene (NB), 4-nitrotoluene (4-NT), 2,4-dinitrotoluene (DNT), 2,4,6-trinitrotoluene (TNT), 4-nitrophenol (PNP) and 2,4,6-Trinitrophenol (PA). Typically, the nanosheet were facilely fabricated by exfoliating the bulk g-C_3N_4 under ultrasonic irradiation (665 W) for 1h, and obtained suspension of g-C_3N_4 nanosheets could be stable in air for several weeks. Remarkably, the nanosheet showed high sensitivity as well as fast response to NACs with the fluorescence quenching rapidly. Significantly, the quenching efficiency coefficient K_{sv} for PNP was 30460 M^{-1}, proving the resultant nanosheets possessed extremely high sensitivity for nitro-phenol PNP detection.

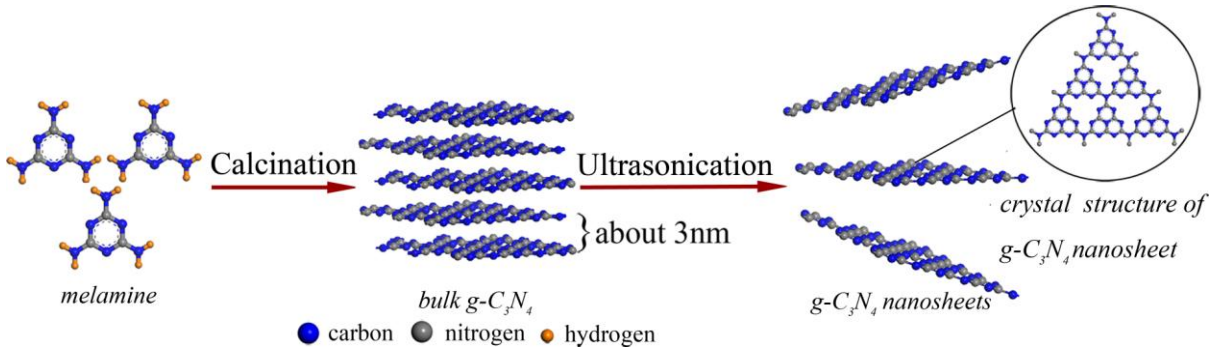

Fig. 1 The schematic illustration for synthesis process of g-C_3N_4 nanosheets.

2. Experimental details

2.1 Materials

Melamine, nitrobenzene (NB), 4-nitrotoluene (4-NT), 2-nitrotoluene (ONT), 2,4-dinitrotoluene (DNT), 2,6-dinitrotoluene (2,6-DNT), 4-nitrophenol (PNP) and 2,4,6-Trinitrophenol (PA) were purchased from Sinopharm (Shanghai) Chemical Reagent Co. Ltd., China. 2,4,6-trinitrotoluene (TNT) standard solution was purchased from J&K Scientific Ltd., China. Other chemicals are

reagent grade quality, and used as received without further purification. Deionized water was used in the experiments.

2.2 Preparation of g-C_3N_4 nanosheets

The suspension of g-C_3N_4 nanosheet was obtained by ultrasonic assisted method, as simulated in Fig. 1. Typically, a certain amount of melamine was put into a crucible with cover and heated to 350 ^oC for 2 h with a heating rate of 5 ^oC / min, then further heated up to 520 ^oC for another 2 h with a heating rate of 20 ^oC / min. After natural cooling to the ambient temperature, the sample (200 mg) was added into 200 mL deionized water containing 50 vol.% THF, and then ultrasound irradiated for 1 h at 665 W ultrasonic power output. The formed suspension was then centrifuged at 6000 rpm to remove the residual un-exfoliated g-C_3N_4 particles. 50 vol.% THF content was determined through experiment, seen supplementary information.

2.3 Characterization

XRD patterns of the as-prepared samples were collected on Philips-1700X diffractometer (Cu-Kα1 radiation, λ=1.54056 Å) using a step scan model from 10°~50°.Transmission electron microscopy (TEM) was obtained on a JEOLJEM-2100 trans-mission electron microscope at 200 kV. Fluorescence spectra were obtained with an excitation wavelength of 308 nm at a Hitachi F-4500 fluorescence spectro-photometer at room temperature. The atomic force microscopy (AFM) study in the present work was performed by means of MultiMode-V (Veeco Metrology, Inc.). X-Ray photoelectron spectra (XPS) analysis was performed on ESCALAB250 spectrometer (Thermo-VG Scientific) using Mg Kα radiation (1253.6 eV) and the binding energy values were calibrated with respect to the C (1s) peak (284.8 eV). The Brunauer-Emmett-Teller surface areas of as prepared samples were analyzed over an ASAP-2020 analyzer at 77 K. The HOMO and LUMO energies were calculated by DMOL3 pakage using the density functional theory (DFT).

For fluorescence sensing of NACs, different contents of nitro aromatic analytes were injected into a 1cm cuvette containing 2 mL as-obtained suspension of g-C_3N_4 nanosheet. The emission intensity was recorded by adding various amount of nitro aromatic compound.

Caution: TNT and PA should be used with extreme caution owing to their high explosion.

3. Results and discussion

The crystal and chemical structure of the g-C_3N_4 nanosheets were analysed by their X-ray diffraction (XRD) patterns, photoluminenscence (PL) emission spectra, and Transmission electron microscopy (TEM) compared with bulk g-C_3N_4. As shown in Fig. 2a, both bulk g-C_3N_4 and the resultant g-C_3N_4 nanosheets have characteristic peak at 27.7°, which can be indexed to the (002) facet caused by the interlayer stacking reflection of conjugated aromatic systems. It is noteworthy that the intensity of the (002) peak decreased significantly in g-C_3N_4 nanosheets compared with the bulk g-C_3N_4, demonstrating the successful exfoliation of bulk g-C_3N_4.[27] The successful exfoliation of bulk g-C_3N_4 was further confirmed by the decreased surface area of the nanosheets. This is consistent with the N_2 sorption-desorption determination (S_{BET} decreased from 18.09 m^2/g to 8.69 m^2/g, and the pore volume decreased from 0.09 cm^3/g to 0.03 cm^3/g). Besides, the photoluminescence spectra of the ultrathin g-C_3N_4 nanosheets show a blue shift of ~4 nm compared with the bulk g-C_3N_4 (Fig. 2b), which indicates a significant change in particle size[28]. The successful exfoliation of bulk g-C_3N_4 was further visualized by the TEM observations. The bulk g-C_3N_4 particles are irregular with size of several micro-meters in length and width. And the electron beam cannot transmit the bulk g-C_3N_4 particles due to its large thickness (Fig. 2c). After 1 h supersonic treatment, very thin g-C_3N_4 products were formed. The size of the as-prepared nanosheets is ~150 nm, which is much smaller and thinner than that of the bulk g-C_3N_4 (Fig. 2d). Unfortunately, the HRTEM image of g-C_3N_4 nanosheets is not attainable due to its

amorphous nature, as evidenced by the selected-area electron diffraction (SAED) analysis (Fig. S2).

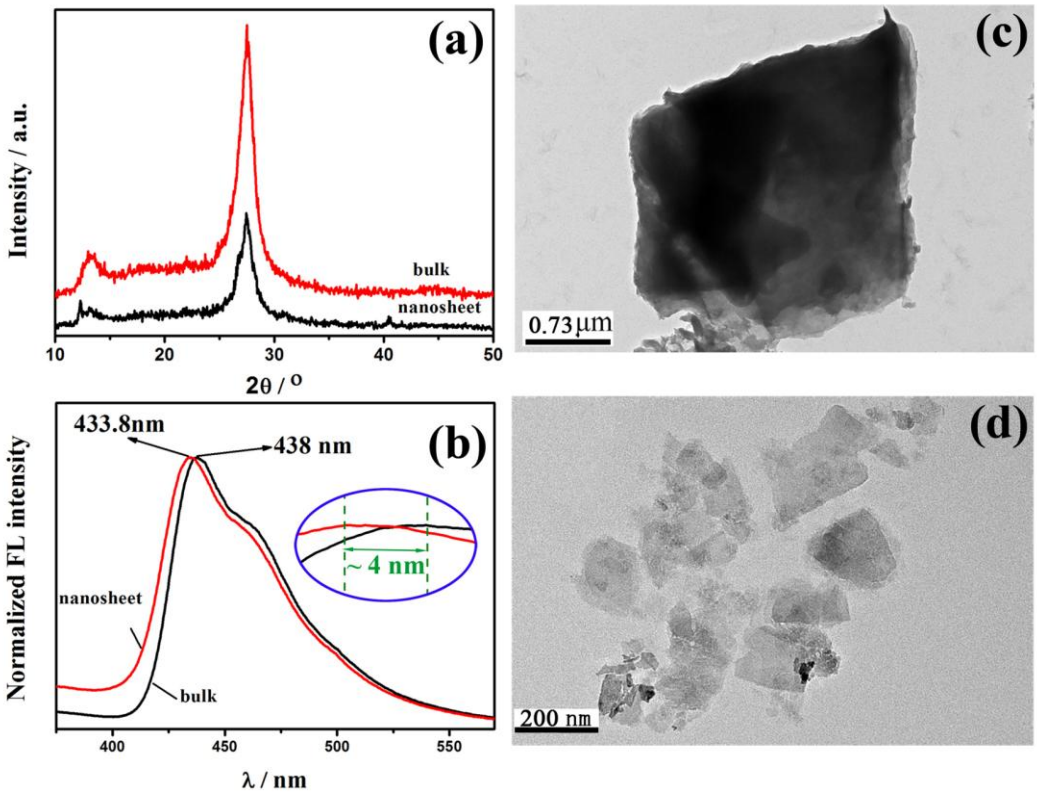

Fig. 2 Comparison of g-C_3N_4 nanosheets and bulk g-C_3N_4 (a) XRD patterns; (b) PL spectra, insert is the enlarged view of the PL peaks; (c) TEM images of bulk g-C_3N_4, and (d) ultrathin g-C_3N_4 nanosheets.

AFM observations were also conducted to verify the successful exfoliation of the bulk g-C_3N_4, as shown in Fig. 3. AFM image shows the nanosheets are well-separated (Fig. 3a) with thickness of ~6-14 nm (Fig. 3b), indicating the successful exfoliation of the bulk g-C_3N_4 into nanosheets with 3~6 C−N layers. The nanosheet nature of g-C_3N_4 was further visualized by high-resolution AFM (HRAFM) observation. Nanosheet with ~6 nm thickness possess relative flat and smooth surface, as revealed by 3D HRAFM image (Fig. 3c, 3d). This result is consistent with the height analysis (Fig. 3b).

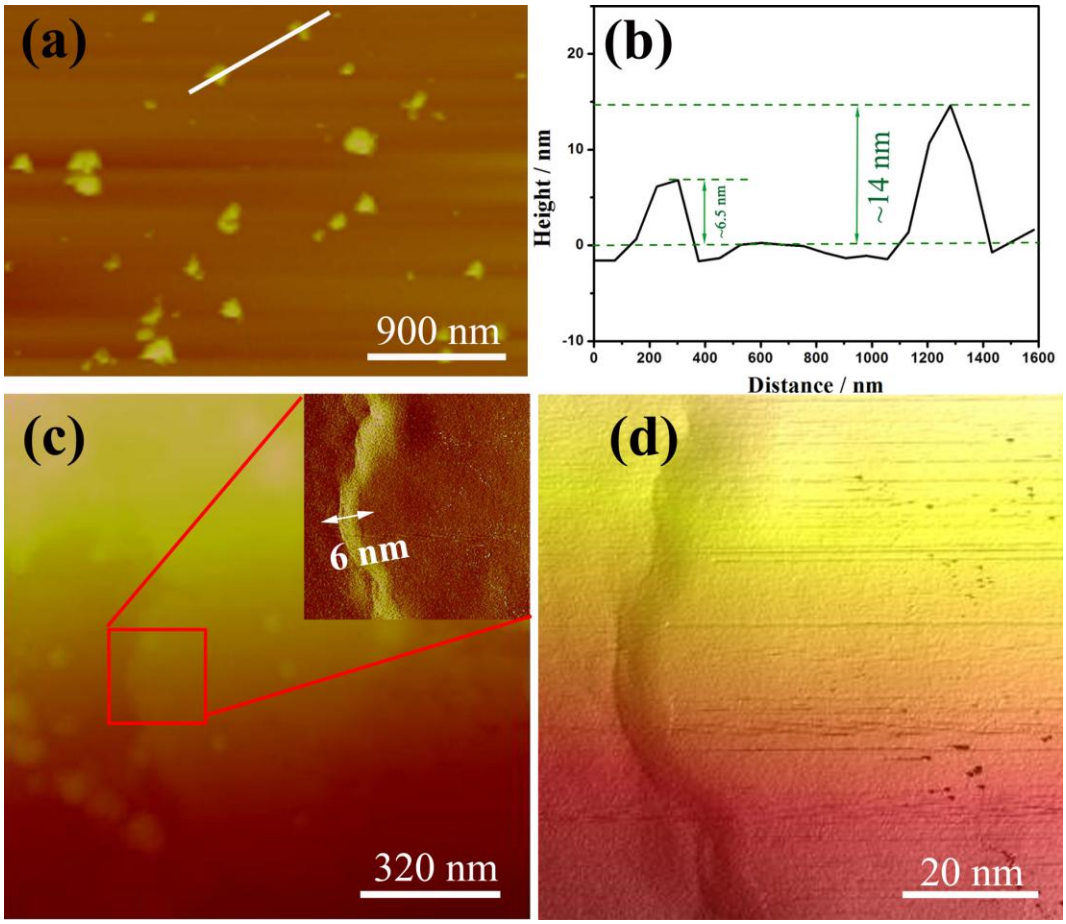

Fig. 3 AFM observation of as-obtained g-C_3N_4 nanosheets. (a) AFM image; (b) Corresponding height analysis; (c) High-resolution AFM image, inset is the magnified image; (d) 3-D image of the inset in Fig. 3c.

To further confirm the structure of the g-C_3N_4 nanosheet, XPS analysis was performed, and the results were shown in Fig. 4. The spectrum in both N 1s and C 1s region could be fitted with three contributions. The C 1s XPS spectrum (Fig. 4a) has three components located at 284.8, 285.7, and 288.0 eV attributed to the C−C bond originated from sp^2 C atoms bonded to N in an aromatic ring (N−C= N), C=N or C≡N ascribed to defect-containing sp^2 hybridized carbon atoms.[29] The N 1s XPS spectrum can be de-convoluted into three peaks centered at 395.7, 397.04, and 398.0 eV (Fig. 4b), corresponding to the sp^2 hybridized aromatic nitrogen atoms bonded to

carbon atoms (C−N=C), tertiary nitrogen N−$(C)_3$ groups linking structural motif or amino groups carrying hydrogen($(C)_2$−NH) related to structural defects, and N−$(C)_3$ groups.[30]

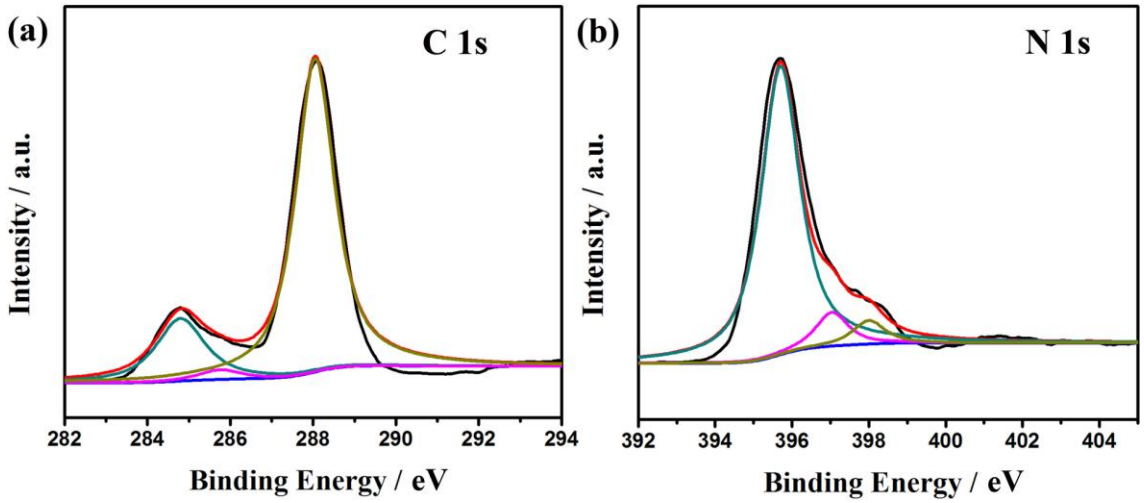

Fig. 4 XPS spectra of the obtained g-C_3N_4 nanosheet in the region of N 1s (a), and C 1s (b).

The prepared g-C_3N_4 nanosheet suspension shows excellent stability, which could be exist in air for several weeks. In addition, g-C_3N_4 nanosheets also possess impressive photo-stability. No obvious change in UV-vis spectra was observed after 1 h full-arc light irradiation (Fig. S3).

g-C_3N_4 nanosheets has strong fluorescence with extremely high quantum yield (QY) up to 32%, benefiting for the inherent fluorescence as well as high QY and stability, the as-obtained nanosheet could be used in detection of NACs with the fluorescence quenching rapidly. Considering most pollutants are usually present in aqueous solution[31], simulating fluorescence sensing property of g-C_3N_4 nanosheets for NACs, such as NB, 4-NT, ONT, DNT, 2,6-DNT, TNT, PNP, and PA was investigated in aqueous solution. As shown in Fig. 5, strong emission peaks at 434 nm can be observed for all of the nitro aromatic analytes, while an evident red-shift emission from 434 to 460 nm occurred when PA concentration increased from 25.6 to 460.8 μM. This phenomenon should be caused by the hydrogen-bond and the strong π-π interaction between PA and g-C_3N_4 nanosheets.[32] As well as the "inner filter effect" of PA, for the reason

that g-C_3N_4 has strong emission peak at 434nm, significantly overlapping with the excitation of PA for PA can absorb in this region (Fig. S4). With the concentration of PA increasing, g-C_3N_4-PA complex occurred and shifted the emission peak from 434 nm to 460 nm. Importantly, strong fluorescence quenching effects were observed for all nitro-aromatics, and fluorescence quenching efficiencies over g-C_3N_4 nanosheets follow the order of PNP > PA » 4-NT > TNT > ONT > DNT ≈ 2,6-DNT ≈ NB. Fluorescence quenching efficiencies exceeded 90% for all analytes with the concentration of NACs increasing, revealing the highly sensitive of the naonosheets to NACs, which might be attributed to the rapid transfer of photo-excited electrons from the excited g-C_3N_4 nanosheets to electron-deficient NACs caused by the strong interaction between g-C_3N_4 and NACs as the strong conjugative effects between triazine rings in g-C_3N_4 nanosheets and aromatic rings in nitro-aromatics, as well as the hydrogen-bond interaction. Besides, in systematic quenching experiments, as one particular size nanosheet quenched first, their contribution to the total emis-sion becomes negligible.[33]

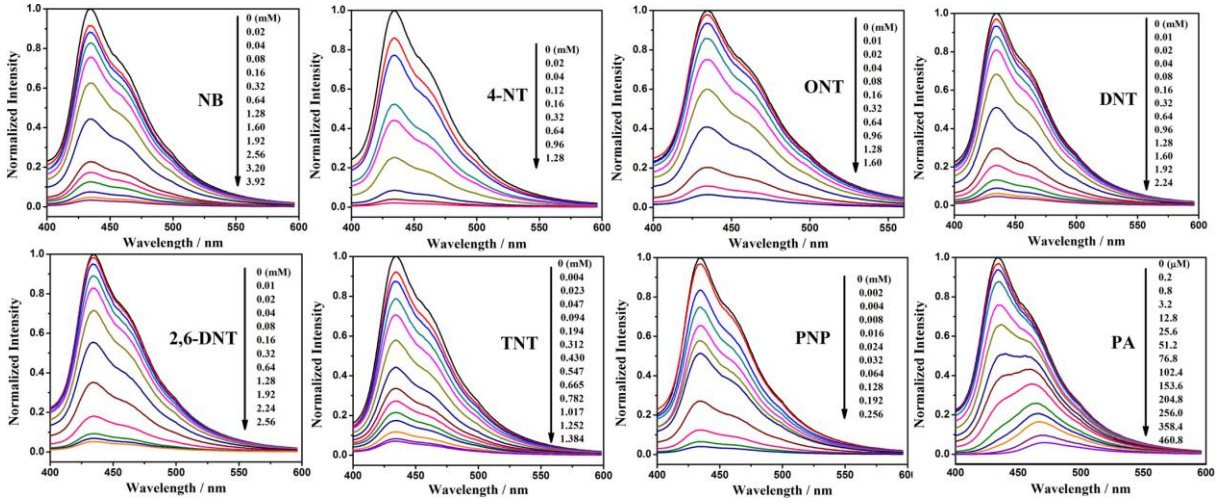

Fig. 5 Fluorescence quenching spectra of g-C_3N_4 nanosheet suspension (2 mL) in the presence of NACs.

The Stern-Volmer constant (K_{sv}) was usually applied to compare the quenching efficiency of various analytes. The Stern-Volmer model is

$$\frac{I_0}{I} = 1 + K_{sv}[M] \quad (1)$$

Where [M] is the analyte concentration (mol/L), I_0 is the fluorescence intensity at [M] = 0, I is the fluorescence intensity at [M], and K_{sv} is the quenching efficiency coefficient of the sensing material.

As shown in Fig. 6, the plots of I_0/I-1 against the NACs concentration are nearly linear. All linear correlation coefficients (R) approach to 1 (Table 1), indicating the fluorescence quenching of the g-C_3N_4 nanosheet suspension caused by target NACs follows the Stern-Vlomer model. The quenching efficiency coefficients K_{sv} for PNP and PA are 30460 and 19390 M^{-1}, respectively, and the results are comparable to that of supramoleculars and surface imprinting polymer (MIP) capped Mn-doped ZnS quantum dots [34,35] In all these K_{sv} values, K_{sv} for PNP and PA are much larger than that of the other analytes, indicating that the g-C_3N_4 nanosheets have extremely sensitivity for NACs detection, especially high selective for nitro-phenols. There are a few of $-NH_2$ in the edge of g-C_3N_4, as we all know. So this result should be attributed to the strong π-π interaction and hydrogen-bond formation between the nanosheets and the hydroxyl of aromatic phenol molecule, as well as proper lowest unoccupied molecular orbital, as will be discussed below.

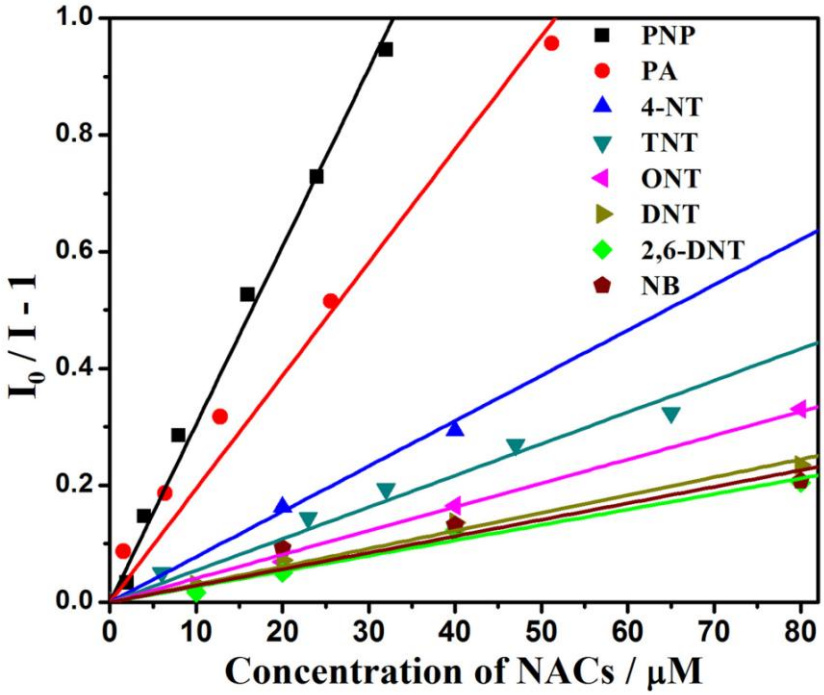

Fig. 6 Stern-Volmer plots of fluorescence quenching of obtained g-C_3N_4 nanosheet suspension (2 mL) in the presence of NACs.

Table 1 Summary of linear correlation coefficients (*R*), quenching efficiency coefficients (K_{sv}) and the standard error of linear fitting.

NACs	*R*	K_{sv} (M^{-1})	Standard error
NB	0.9606	2820	2.846E-4
2,6-DNT	0.9906	2650	1.155E-4
DNT	0.9936	3060	1.099E-4
ONT	0.9951	4080	1.272E-4
TNT	0.9895	5420	2.277E-4
4-NT	0.9994	7760	8.829E-5
PA	0.9878	19390	8.729E-4
PNP	0.9964	30460	6.908E-4

To further investigate the selectivity to NACs, a quantitative quenching experiment was carried out, in which 256 μM was the upper limit concentration of the NACs (NB, 4-NT, ONT, DNT, 2,6-DNT, TNT, PNP and PA), as shown in Fig. 7. It can be found that the PL intensity decreased with the presence of NACs, which proved that the g-C_3N_4 nanosheets are sensitive to NACs. Typically, the fluorescence quenched rapidly especially with the presence of PNP, and the fluorescence quenching efficiencies exceeded 90% with the concentration of PNP up to 256 μm, and this indicates that g-C_3N_4 nanosheet was particularly high selective to PNP. And the g-C_3N_4 nanosheet might be used as promising fluorescence probes for PNP detection.

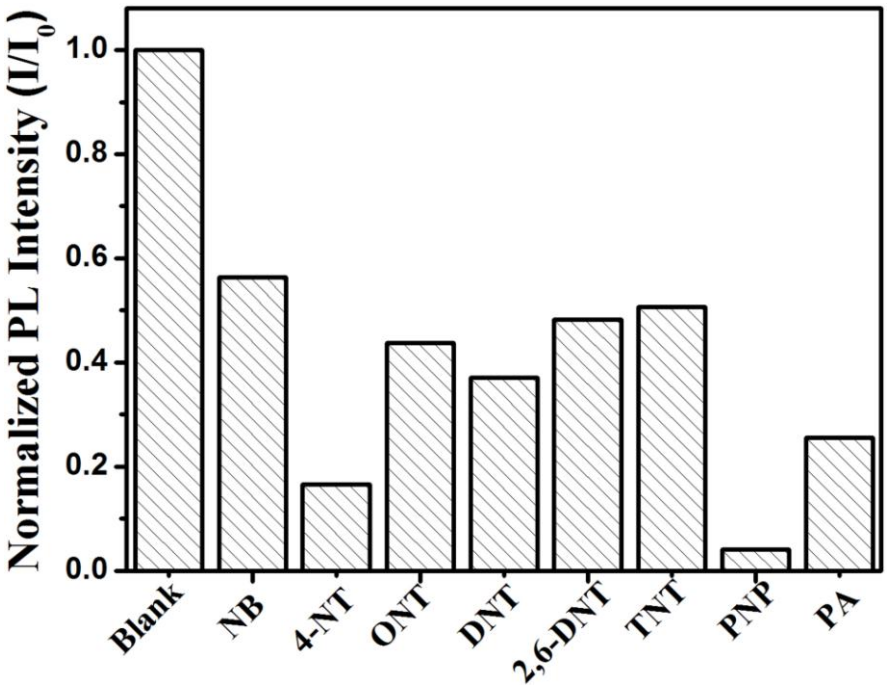

Fig. 7 The difference in normalized PL intensities of g-C_3N_4 nanosheet suspension (2 mL) at 434 nm between the blank and suspension containing different NACs (excitated at 308 nm, [NACs] = 256 μM, I and I_0 are the PL intensities of g-C_3N_4 nannosheet suspension in the presence and absence of NACs, respectively).

In order to get insight of the sensing mechanism, time resolved fluorescence of the nanosheet was investigated (Fig. S5). With the time increasing, no obvious fluorescence quenching was observed. That is fluorescence of the g-C_3N_4 nanosheet would not quench itself naturally. Based on all these experimental results, a sensing mechanism for NACs by g-C_3N_4 nanosheets was tentatively proposed, as illustrated in Fig. 8, in which NB was chose as the target nitro aromatic explosive. g-C_3N_4 nanosheet has big conjugated structure, rigid planes, and a few of electron-donating group $-NH_2$, so it has high performance of photoluminenscence. As the explosive NB was added into the g-C_3N_4 nanosheet suspension, on the one hand NB could impact with the fluorescent nanosheet, so as lead to some fluorescent quenching on the bases of energy transduction or charge transfer mechanism. And this is called dynamic quenching. On the other hand, the primary-networks of the g-C_3N_4 nanosheets can act as receptors for NB molecules over the strong-interaction and electrostatic adhesion, and the resulted molecular has no fluorescence in the detected spectral region. And this is called static quenching.[36] In addition, the proper energy levels promote the excited state electrons transfer from the nanosheet to analyte NACs, which might be responsible for the sensitive response. The LUMO and HOMO orbital energy of the tested NACs were calculated (Fig. S6). All the LUMO energy of the NACs was lower than that of g-C_3N_4 nanosheet, and they are expected to represent how easily electrons can be transferred to the electron-deficient analyte in the fluorescence quenching process.[37, 38] The LUMO energy was in the sequence of PA > PNP > 4-NT ≈ TNT ≈ ONT > DNT ≈ 2,6-DNT ≈ NB, which is roughly close to the order of their quenching efficiency in the sensing experiments, indicating that the photo-induced electron transfer is not the only mechanism for the quenching, as expounded above.

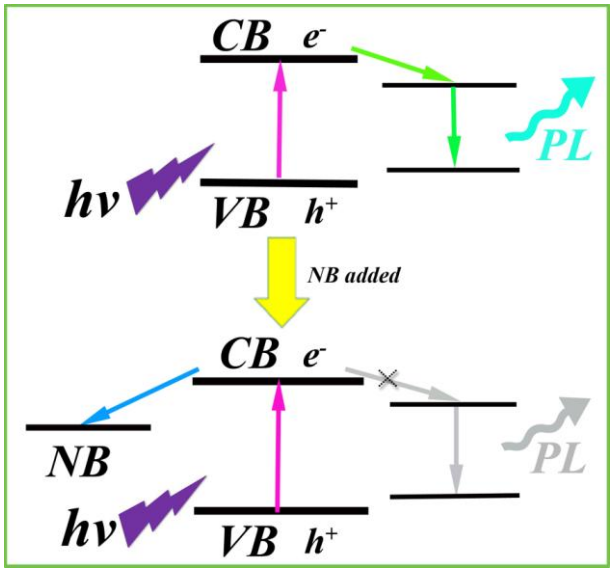

Fig. 8 Suggested schematic illustration of the g-C_3N_4 nanosheet for detection of NACs.

4. Conclusion

In conclusion, the g-C_3N_4 nanosheets were successfully prepared by exfoliating the bulk g-C_3N_4 in water assisted by ultrasonic method. And their application for detection of nitro aromatic explosives was demonstrated. Particularly, luminescence property of the as-prepared nanosheet was found to be sensitive to nitro aromatic explosives, especially selective to nitro-phenol PNP. The results presented in this work demonstrated a new application of g-C_3N_4, and the g-C_3N_4 nanosheet may be further extended to the applications in biomarker and biomedicine due to its high quantum yield (32%) and stability.

Acknowledgments

This work was financially supported by the National Natural Science Foundation of China (21371002), Anhui Provincial Natural Science Foundation (1408085MB22).

References

1 M. A. Ivy, L. T. Gallagher, A. D. Ellington and E. V. Anslyn, *Chem. Sci.*, 2012, **3**, 1773-1779.

2 N. Dey, S. K. Samanta and S. Bhattacharya, *ACS Appl. Mater. Interfaces*, 2013, **5**, 8394-8400.

3 K. J. Albert and D. R. Wal, *Anal. Chem.*, 2000, **72**, 1947-1955.

4 A. Rose, Z. G. Zhu, C. F. Madigan, T. M. Swager and V. Bulovic, *Nature,* 2005, **434**, 876-879.

5. F. Monteil-Rivera, C. Beaulieu, S. Deschamps, L. Paquet and J. Hawari, *J. Chromatogr. A*, 2004, **1048**, 213-221.

6 S. J. Toal and W. C. Trogler, *J. Mater. Chem*., 2006, **16**, 2871-2883.

7 S. Shanmugaraju,S. A. Joshi and P. S. Mukherje, *J. Mater. Chem.*, 2011, **21**, 9130-9138.

8 J. B. Liu, X. H. Yang, X. X. He, K. M. Wang, Q. Wang, Q. P. Guo, H. Shi, J. Huang and X. Q. Huo, *Sci. China Chem.*, 2011, **54**, 1157-1176.

9 G. Y. Wang, L. L. Yang, H. Song, W. J. Ruan, Z. Chang and X. H. Bu, *Dalton Trans.*, 2013, **42**, 12865-12868.

10 J. A. Greathouse, N. W. Ockwig, L. J. Criscenti, T. R. Guilinger, P. Pohl, and M. D. Allendorf, *Phys. Chem. Chem. Phys.*, 2010,**12**, 12621-12629

11 W. Zou, W. W. Liu, L. M. Luo, S. F. Zhang, R. W. Lu and G. Veser, *J. Mater. Chem.*, 2012, **22**, 12474-12478.

12 L. S. Fan, Y. W. Hu, X. Wang, L. L. Zhang and F. H. Li, *Talanta*, 2012, **101**, 192-197.

13 H. Y. Chen, L. G. Qiu, J. D. Xiao, S. Ye, X. Jiang and Y.P. Yuan, *RSC Adv.*, 2014, **4**, 22491-22496.

14 L. M.Sun, X. Zhao, C. J. Jia, Y. X. Zhou, X. F. Cheng, P. Li, L. Liu and W. L. Fan, *J. Mater. Chem.*, 2012, **22**, 23428-23438.

15 J. Q. Tian, R. Ning, Q. Liu, A. M. Asiri, A. O. Al-Youbi and X. P. Sun, *ACS Appl. Mater. Interfaces*, 2014, **6**, 1011-1017.

16 J. Q. Tian, Q. Liu, A. M. Asiri, K. A. Alamry and X. P. Sun, *ChemSusChem*, 2014, **7**, 2125-2132.

17 X. D. Zhang, X. Xie, H. Wang, J. J. Zhang, B. C. Pan and Y. Xie, *J. Am. Chem. Soc.*, 2013, **135**, 18-21.

18 J. Q Tian, Q. Liu, C. J. Ge, Z. C. Xing, A.M. Asiri, A. O. Al-Youbi and X. P. Sun, *Nanoscale*, 2013, **5**, 8921-8924.

19 J. Q. Tian, Q. Liu, A. M. Asiri, A. H. Qusti, A. O. Al-Youbi and X. P. Sun, *Nanoscale*, 2013, **5**, 11604-11609.

20 N. Y. Cheng, P. Jiang, Q. Liu, J. Q. Tian, A. M. Asiri and X. P. Sun, *Analyst*, 2014, **139**,5065-5068.

21 J. Q. Tian, Q. Liu, A. M. Asiri, A. O. Al-Youbi and X. P. Sun, *Anal. Chem.*, 2013, **85**, 5595-5599.

22 M. Groenewolt and M. Antonietti, *Adv. Mater.*, 2005, **17**, 1789-1792.

23 M. R. Jameia, M. R. Khosravi and B. Anvaripour, *Ultrason. Sonochem.*, 2014, **21**, 226-233.

24 M. P. Neupane, I.S. Park, T. S. Bae and M. H. Lee, *J. Alloys Compd.*, 2013, **581**, 418-422.

25 J. C. Yu, J. Yu, W. Ho and L. Zhang, *Chem. Commun.*, 2001, **6**, 1942-1943.

26 J. J. Qian, L. G. Qiu, Y. M. Wang, Y. P. Yuan, A. J. Xie and Y. H. Shen, *Dalton Trans.*, 2014, **43**, 3978-3983.

27 S. B. Yang, Y. J. Gong, J. S. Zhang, L. Zhan, L. L. Ma, Z. Y. Fang, R. Vajtai, X. C. Wang and P. M. Ajayan, *Adv. Mater.*, 2013, **25**, 2452-2456.

28 L. C. Chen, D. J. Huang, S. Y. Ren, T. Q. Dong, Y. W. Chi and G. N. Chen, *Nanoscale*, 2013, **5**, 225-230.

29 S. Z. Hu, L. Ma, J. G.You, F. Y. Li, Z. P. Fan, G. Lu, D. Liu and J. Z. Gui, *Appl. Surf. Sci.*, 2014, **311**, 164-171.

30 X. Y. Li, Y. Wang, L. H. Kang, M. Y. Zhu, B. Dai, *J. Catal.*, 2014, 311, 288-294.31 M. R. Fanny, C. Beaulieu, S. Deschamps, L. Paquet and J. Hawari, *J. Chromatogr. A*, 2004, **1048**, 213-221.

31 M. R. Fanny, C. Beaulieu, S. Deschamps, L. Paquet and J. Hawari, *J. Chromatogr. A*, 2004, **1048**, 213-221

32W. Zhang, L. G. Qiu, Y. P. Yuan, A. J. Xie, Y. H. Shen and J. F. Zhu, *J. Hazard. Mater.*, 2012, **221-222**, 147-154.

33T. Pazhanivel, D. Nataraj,V. P. Devarajan, V. Mageshwari, K. Senthil and D. Soundararajan, *Anal. Methods*, 2013, **5**, 910-916.

34 M. E. Germain, M. Knapp, *Chem. Soc. Rev.,* 2009, **38**, 2543-2555.

35 X. J. Liu, H. Chen, Z. Lin and J. M. Lin, *Anal. Chem.,* 2010, **82**, 7380-7386.

36 Wuhan University, Analytical Chemistry, Higher Education Press: Beijing, China, 2012, **vol. 2**, ch. 8, pp. 211-216.

37 S. S. Nagarkar, B. Joarder, A. K. Chaudhari, S. Mukherjee and S. K. Ghosh, *Angew. Chem.,* 2013, **125**, 2953-2957.

38 J. Y. Zhang, Y. H. Wang, J. Jin, J. Zhang, Z. Lin, F. Huang and J. G. Yu, *ACS Appl. Mater. Interfaces*, 2013, **5**, 10317-10324.

Table of contents entry

Ultrasonic assisted synthesised strong fluorescence g-C_3N_4 nanosheets with quantum yield up to 32% for trace level explosives sensing.